Power Law Correlations for Lift from Direct Numerical Simulation of Solid-Liquid Flow

Daniel D. Joseph
Department of Aerospace Engineering and Mechanics
107 Akerman Hall, 110 Union Street SE
University of Minnesota
Minneapolis, MN 55455

(612) 625-0309 office; (612) 625-1558 fax

E-mail: *joseph@aem.umn.edu*

http://www.aem.umn.edu/Solid-Liquid_Flows

March, 2001

Abstract

Lift forces acting on a fluidized particle plays a central role in many important applications, such as the removal of drill cuttings in horizontal drill holes, sand transport in fractured reservoirs, sediment transport and cleaning of particles from surfaces. The problem of lift is studied using direct numerical simulations. Lift formulas which respect the fact that the lift must change sign on either side of the "Segré-Silberberg" radius are discussed. An accurate analytical expression for the slip velocity of circular particles in Poiseuille flow is derived. We show that the lift-off of single particles and many particles in horizontal flows follow laws of similarity, power laws, which may be obtained by plotting simulation data in 2D on log-log plots. Data from slot experiments on bed erosion for fractured reservoirs is processed (for the first time) in log-log plots. Power laws with a parameter dependent power emerge as in the case of Richardson-Zaki correlations for bed expansion.

Preface

My collaborators on studies of lift are H. Choi, H. Hu, P. Huang, T. Ko, D. Ocando, N. Patankar and P. Singh. This is but one aspect of a concentrated NSF supported study of direct numerical simulations of solid-liquid flow. The results of such studies are collected at the project web site *http://www.aem.umn.edu/Solid-Liquid_Flows*. The whole field is reviewed in the monograph under preparation "Interrogation of Direct Numerical Simulations of Solid-Liquid Flow," which can be downloaded from the web site *http://www.aem.umn.edu/Solid-Liquid_Flows/papers/abs_Interrogation.html*.

Direct numerical simulation (DNS) of solid-liquid flow.

The current popularity of computational fluid dynamics is rooted in the perception that information implicit in the equations of fluid motion can be extracted without approximation using direct numerical simulation (DNS). A similar potential for solid-liquid flows, and multiphase flows generally, has yet to be fully exploited, even though such flows are of crucial importance in a large number of industries.

We have taken a major step toward the realization of this potential by developing two highly efficient parallel finite-element codes called *particle movers* for the direct numerical simulation of the motions of large numbers of solid particles in flows of Newtonian and viscoelastic fluids. One of the *particle movers* is based on moving unstructured meshes (arbitrary Lagranian-Eulerian or ALE) and the other on a structured mesh (distributed Lagrange multiplier or DLM) using a new method involving a distribution of Lagrange multipliers to ensure that the regions of space occupied by solids are in a rigid motion. Both methods use a new combined weak formulation in which the fluid and particle equations of motion are combined into a single weak equation of motion from which the hydrodynamic forces and torques on the particles have been eliminated. Several different kinds of code have been developed and tried on a variety of applications. See the project Web site, *http://aem.umn.edu/Solid-Liquid_Flows/*. To our knowledge we are the only group to compute fully resolved particulate flow at Reynolds numbers in the thousands occurring in the applications.

Richardson and Zaki (RZ) correlations.

The correlations of Richardson and Zaki (1954) (see also Pan, Joseph, Bai, Glowinski and Sarin 2001) are an empirical foundation for fluidized bed practice. They did very many experiments with different liquids, gases, particles and fluidization velocities. They plotted their data in log-log plots; miraculously this data fell on straight lines whose slope and intercept could be determined. This showed that the variables follow power laws; a theoretical explanation for this outstanding result has not been proposed. After processing the data Richardson and Zaki found that

$$V(\phi) = V(0)\,(1-\phi)^n$$

where $V(\phi)$ is the composite velocity which is the volume flow rate divided by the cross-section area at the distributor when spheres of volume fraction f are fluidized by drag. $V(0)$ is the "blow out" velocity, when $\phi = 0$; when $V > V(0)$ all the particles are blown out of the bed. Clearly $V(\phi) < V(0)$. The RZ exponent $n(R)$ depends on the Reynolds number $R = V(0)d/\nu$; $n = 2.39$ when $500 < R < 7000$.

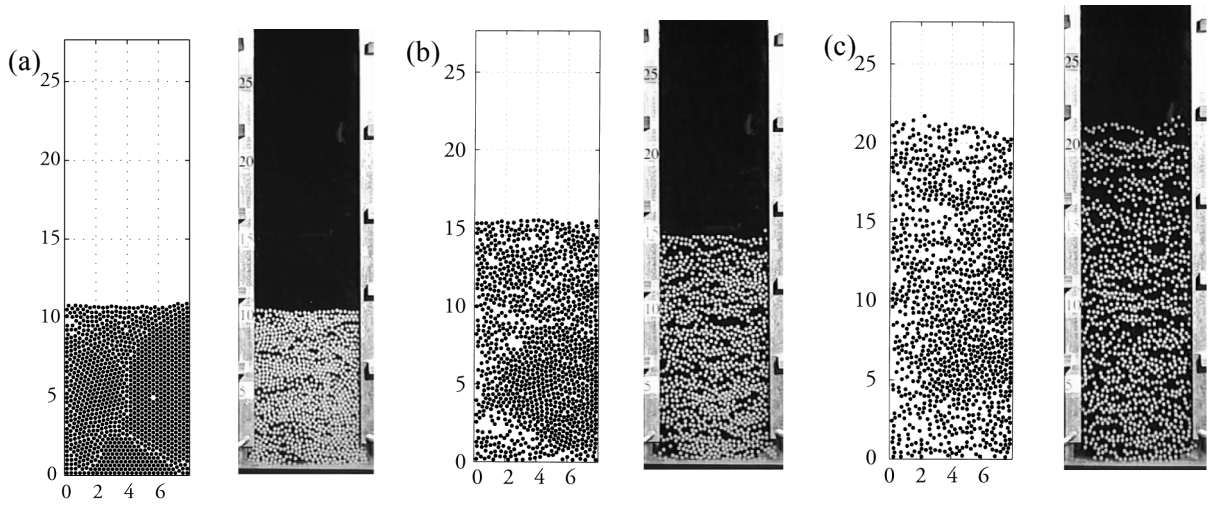

(a)
- V = 2 : Particle position at t = 5.625.
- The maximal particle Reynolds number is 1383.
- The maximal averaged particle Reynolds number is 130.

(b)
- V = 3.5 : Particle position at t = 17.238
- The maximal particle Reynolds number is 1671.
- The maximal avaraged particle Reynolds number is 236.

(c)
- V = 4.5 : Particle position at t = 31.
- The maximal particle Reynolds number is 1859.
- The maximal averaged particle Reynolds number is 292.

Figure 1. (Pan, Joseph, Bai, Glowinski and Sarin 2001). Snapshots of fluidization of 1204 spheres comparing experiment (right) and simulation (left) (a) V = *2, (b)* V = *3.5, (c)* V = *4.5.*

We carried out DNS simulations of 1204 balls in a slit bed whose dimensions exactly match a real experiment. The simulation is compared with a matched real experiment and they give rise to essentially the same results (see figure 1). This simulation is presently at the frontier of DNS; it is a 3D computation of 1204 spheres at Reynolds numbers based on the sphere diameter of the order of 10^3 and the agreement with experiment is excellent. The details and animation of the computation (Pan, *et al* 2001) can be found at *http://www.aem.umn.edu/Solid-Liquid_Flows*.

The simulation of 1204 spheres was carried out in the bed [depth, width, height] = [0.686, 20.30, 70.22] cm. Snapshots comparing the animation with the experiment, in a frontal view are shown in figure 1. Figure 2 shows the fluidizing velocity vs. liquid fraction ε in a log-log plot; one line is for the simulation and another for the experiment. We draw a straight line with slop $n = 2.39$ through both sets of data. The fit is not perfect but we think rather encouraging. From the straight lines we determine the blow-out velocities $V_s(0) = 8.131$ cm/s for the simulation and $V_e(0) = 10.8$ cm/s for the experiment, and find the power laws

$$V_s(\phi) = 8.131\varepsilon^{2.39}\ \text{cm/s} \tag{1}$$

Pan, *et al* (2001) presented arguments that the discrepancy is due to the difference in the diameter 0.635cm of the sphere in the simulation and the average diameter 0.6398cm of the 1204 spheres uses in the experiments.

$$V_e(\phi) = 10.8\varepsilon^{2.39}\ \text{cm/s}\ .$$

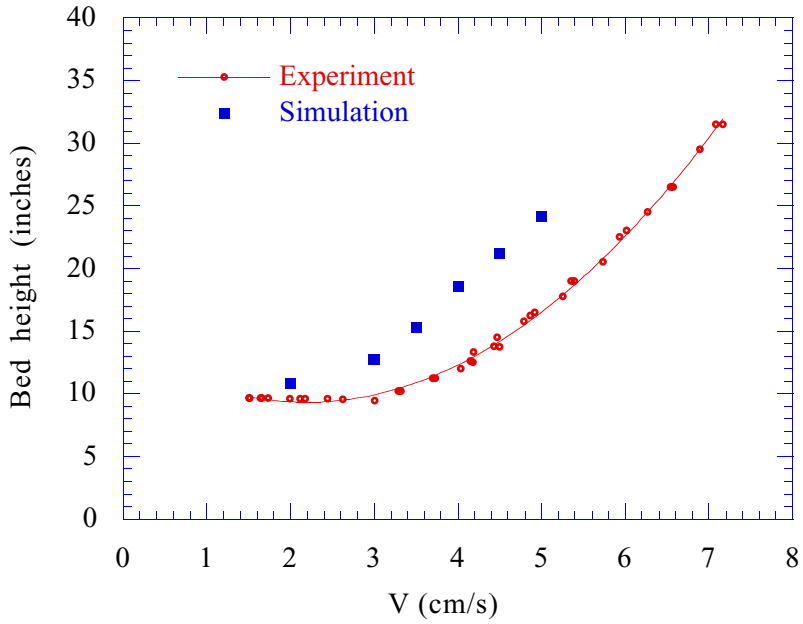

Figure 2(a). (Pan, et al 2001) The bed height vs. fluidizing velocity for both experiment and simulation.

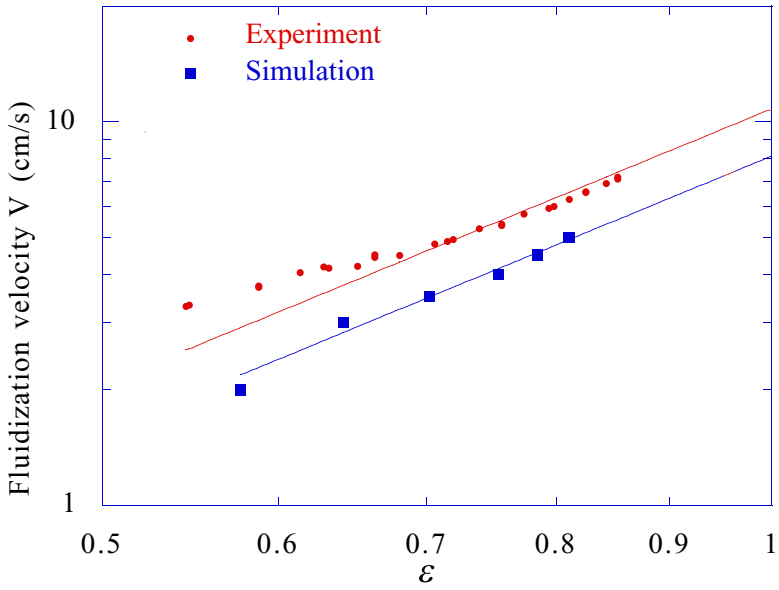

Figure 2(b). Data from Figure 2(a) plotted in a log-log plot. The slopes of the straight line are given by the Richardson-Zaki n = *2.39. The blow-out velocities* $V_s(0)$ *and* $V_e(0)$ *are defined as the intercepts at* $\varepsilon = 1$.

Single particle lift off and levitation to equilibrium.

The problem of lift off and levitation to equilibrium of a single circular particle in a plane Poiseuille flow was simulated using an ALE particle mover in Patankar, Huang, Ko and Joseph (2001). The principal features of lift off and levitation to equilibrium are listed in the caption of figure 3. Heavier particles are harder to lift off. The critical lift off Reynolds number increases strongly with the density ratio. The height, velocity and angular velocity of the particle at equilibrium is given as a function of prescribed parameters in tables and trajectories from lift-off to equilibrium in graphs shown in Patankar, *et al* (2001).

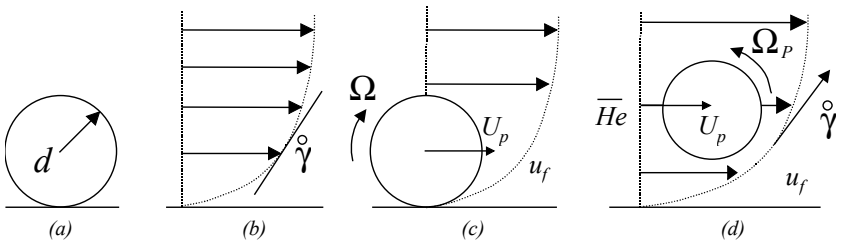

Figure 3. Lift off and levitation to equilibrium. The pressure gradient in the flow and on the particle is increased. The heavier than liquid particle slides and rolls on the bottom of the channel. At a critical speed the particle lifts off. It rises to a height in which the lift balances the buoyant weight. It moves forward without acceleration at a steady velocity and angular velocity.

The channel height is W, particle diameter d, density of fluid ρ_f and particle ρ_p, viscosity η, kinematic viscosity η/ρ_f . The equation of motion of fluid and particles made dimensionless with $[d,w,d/v,\eta\dot{\gamma}_w]$ where $\dot{\gamma}_w$ is the wall shear rate and $\overline{p}$ is the applied pressure gradient that drives the flow, are in the form

$$\textit{Solid}\ \begin{cases} R\left[\dfrac{\partial \mathbf{u}}{\partial t}+\mathbf{u}\cdot\nabla\mathbf{u}\right]=-\nabla p+2\dfrac{d}{w}\mathbf{e}_x+\nabla^2\mathbf{u}, & (2)\\[2ex] \dfrac{\rho_p}{\rho_f}R\dfrac{d\mathbf{U}}{dt}=-\dfrac{R_G}{R}e_y+2\dfrac{d}{w}\mathbf{e}_x+\dfrac{4}{\pi}\int_0^{2\pi}\left(-p+2\mathbf{D}[\mathbf{u}]\right)\cdot\mathbf{n}d\theta & (3)\\[2ex] \dfrac{\rho_p}{\rho_f}R\dfrac{d\mathbf{U}}{dt}=-\dfrac{R_G}{R}e_y+2\dfrac{d}{w}\mathbf{e}_x+\dfrac{4}{\pi}\int_0^{2\pi}\left(-p+2\mathbf{D}[\mathbf{u}]\right)\cdot\mathbf{n}d\theta\,. & (4)\end{cases}$$

The flow is determined by four dimensionless groups,

$$\frac{\rho_p}{\rho_f},\ \frac{2d}{w},\ R=\frac{\rho_f\gamma_w d^2}{\eta},\ R_G=\frac{\rho_f\left(\rho_p-\rho_f\right)gd^2}{\eta^2} \tag{5}$$

where R is the shear Reynolds number and R_G is a Reynolds number based on the sedimentation velocity in Stokes flow. The terms with the factor $\mathbf{e}_x$ come from the pressure gradient; the pressure gradient ($2d\mathbf{e}_x/w$ in (3)) drives the particle forward and the forward motion is resisted by the integral of the shear tractions.

Freely moving particles in steady flow have zero acceleration. The density ratio ρ_p/ρ_f vanishes when the particle accelerations are zero.

The critical value of the Reynolds number for lift-off increases with density of the particle from zero for neutrally buoyant $\rho_p = \rho_p$ circular particles to R = 25 for particles 1.4 times heavier than water ρ_p = 1.4 ρ_f. After the particle lifts off it rises to an equilibrium height in which the buoyant weight equals the hydrodynamic lift. The equilibrium height for neutrally buoyant particles is called a "Segré-Silberberg" radius; it is determined by a balance of wall and shear gradient effects. The equilibrium height for heavy particles is lower than the Segré-Silberberg height. The rise to equilibrium is shown in figure 4.

DNS results given in Patankar, Huang, Ko and Joseph (2001) show that a circular particle will rise higher when the rotation of the particle is suppressed and least when the slip angular velocity is put to zero; the freely rotating zero torque case lies between. DNS allows such a comparison, which would be difficult or impossible to carry out in an experiment.

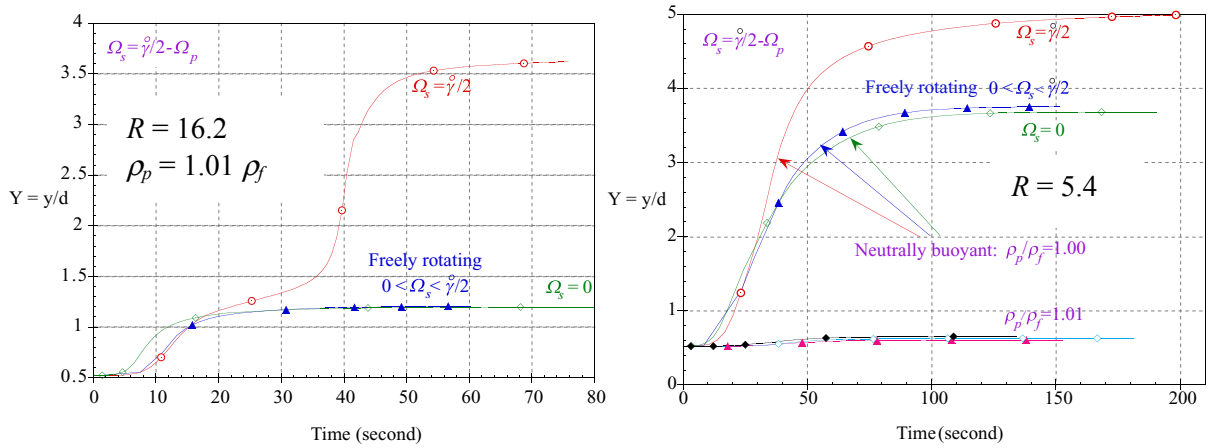

Figure 4. (Patankar, Huang, Ko and Joseph 2001.) Rise vs. time for R_w = 16.2 and 5.4. Compare rise of freely rotating and nonrotating particles. Nonrotating ones rise more. A neutrally buoyant, freely rotating particle rises closer to the center line than the "Segré-Silberberg" experiment; the nonrotating one rises even more. Models which ignore particle rotation overestimate lift. A yet smaller lift is obtained when the slip velocity is entirely suppressed (Ω_s = 0), but the particle does rise. The greater the slip angular velocity, the higher the particle will rise.

Slip velocities, circulation and lift.

In commercial packages for slurry flow in pipes, conduits and fractured oil and gas reservoirs, lift forces are not modeled, and in academic studies they are not modeled well. Possibly the best known and most used formula for lift is the Rayleigh Formula $L = \rho_f U \Gamma$ for aerodynamic lift. Here U is the forward velocity in still air that is produced by an external agent like a rocket engine, and Γ is the circulation, which is a complicated quantity determined by boundary layer separation. The lift on a free body in a shear flow is analogous and the lift formulas that have been proposed are in the form of U_s, the slip velocity, times $\rho_f \Gamma$, where Γ is a different quantity for different modelers. The slip velocity is the fluid velocity at the particle center when there is no particle minus the particle velocity. Since it is the fluid motion rather than an external agent which drives the motion of the particle, it might be expected that $U_s > 0$. Since free particles in shear flow migrate to an equilibrium radius, the associated Γ ought to change sign at this radius; in fact none of the lift formulas that have been proposed do change sign; if they are right at one side of the equilibrium they are wrong on the other. The slip angular velocity discrepancy defined as the difference between the slip angular velocity of a migrating particle and the slip angular velocity at its equilibrium position is positive below the position of equilibrium and negative above it. This discrepancy is the quantity that changes sign above and below the equilibrium position for neutrally buoyant particles, and also above and below the lower equilibrium position for heavy particles. On the other hand the slip velocity discrepancy U_s - U_{se} does not change sign Joseph, Ocando and Huang (2001).

Model of slip velocity.

A long particle model was proposed in Joseph, Ocando and Huang (2001), which leads to an explicit expression for the particle velocity U_p of a circular particle in a Poiseuille flow. Referring to Figure 5 we find that

$$U_A = \phi + \psi h_A d, \quad U_B = \phi + \psi h_B d \tag{6}$$

where

$$\phi = \frac{\bar{b}}{\eta}(2d + h_A + h_B)h_A h_B / 2(h_A + h_B)$$

$$\psi = \overset{\circ}{\gamma}(h_B + d/2) \Big/ 2(h_A + h_B)$$

and the particle velocity U_p is given by

$$U_p = \overset{\circ}{\gamma}\ (U_A + U_B)/2.$$

The slip velocity U_s is given by

$$U_s = \frac{\bar{p}}{2\eta}\left(h_B + \frac{d}{2}\right)\left(h_A + \frac{d}{2}\right) - U_p > 0 \quad \text{and} \quad U_s = 0 \quad \text{when} \quad d = 0. \tag{7}$$

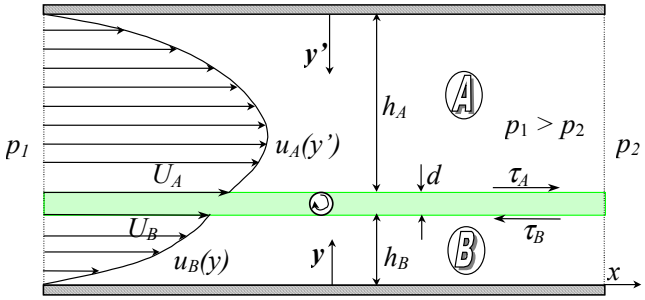

Figure 5. (Joseph, Ocando and Huang 2001.) The circular particle is replaced with a long rectangle where short side is d. The rectangle is so long that we may neglect the effects of the ends of the rectangle at sections near the rectangle's center. The rectangle is sheared at the shear rate of the circular particle $\Omega_p \cong \dot{\gamma}/2$ *(see Figure 4). The velocity profile is Poiseuille flow on either side of the particle and* U_A *and* U_B *determined by requiring that the pressure gradient* $\bar{p}$ *balance the shear stress.*

A comparison of the velocity profile of the long particle model with the velocity profile through the center of the circular particle computed by direct numerical simulation is given in Figure 6. Such a good agreement is surprising.

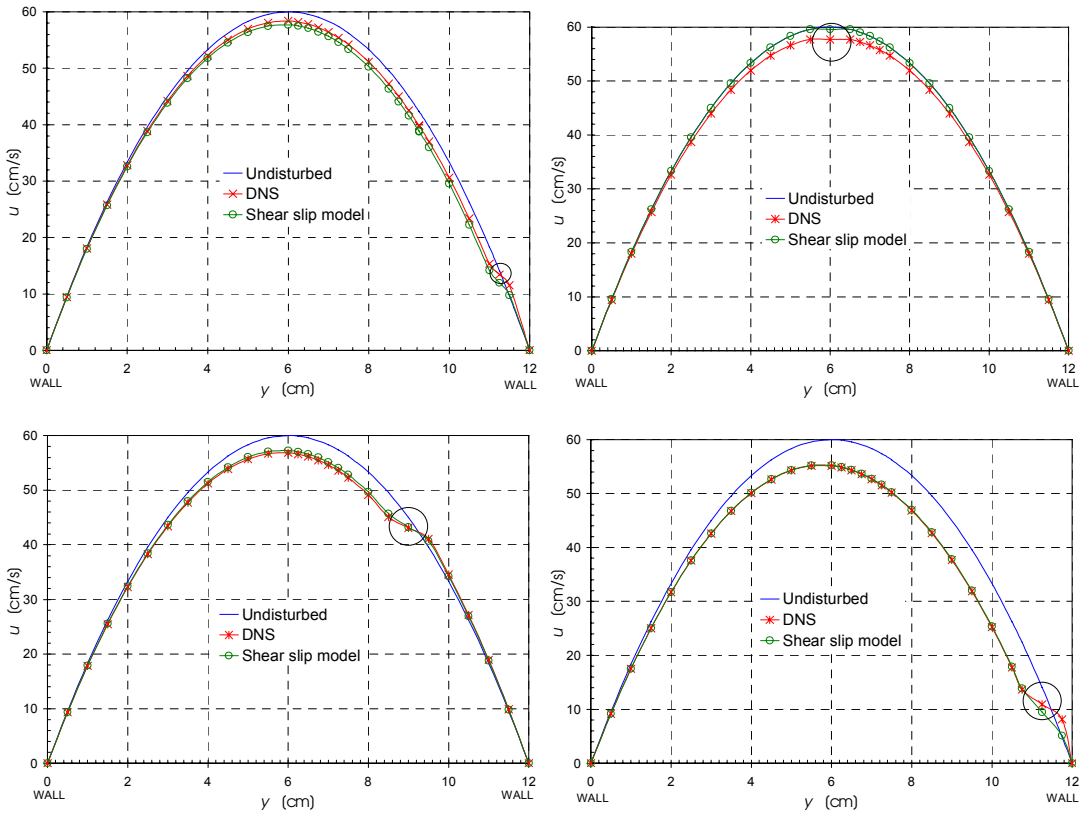

Figure 6. (Joseph, Ocando and Huang 2001.) Comparison of the velocity profiles (Figure 5.) for the long particle model with the velocity profile on a line through the circular particle center computed by DNS for constrained motion at R = 20. In a constrained motion the y position of the particle is fixed, lateral motion is suppressed, but the particle is otherwise free to translate and rotate under the action of the hydrodynamic forces and torques.

Bifurcation.

A turning point bifurcation of steady forward flow of a single particle at equilibrium was found in direct simulations of rise trajectories reported in Choi and Joseph (2001); the height and particle velocity change strongly at such a point. A computational method advanced in Patankar, Huang, Ko and Joseph (2001) looks for the points on lift vs. height curve at which lift balances buoyant weight. This gives both stable and unstable solutions and leads to the "bifurcation" diagram shown in Figure 7, which shows there are two turning points, hysteresis, but no new branch points.

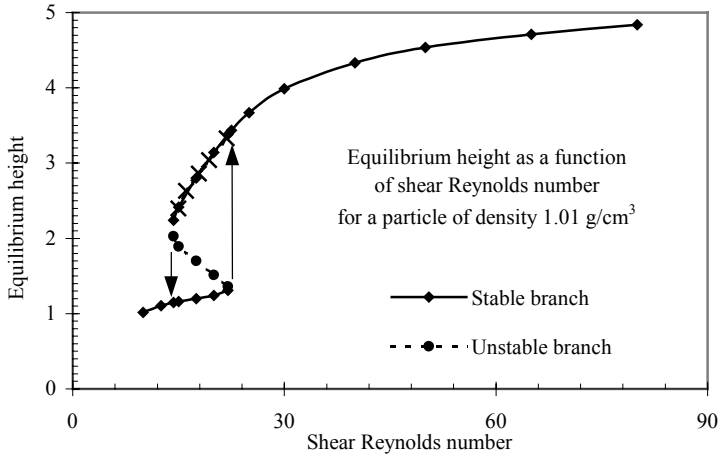

Figure 7. (Patankar, Huang, Ko and Joseph 2001.) Turning point "bifurcations" shown in the height vs. Reynolds number curve. There are two stable branches separated by an unstable branch.

Similar turning point bifurcations have been found also in computations of levitation to equilibrium of viscoelastic fluids of Oldroyd-B type. Similar instabilities have been found at yet higher Reynolds numbers. Bifurcations of sedimenting particles, including Hopf bifurcations to periodic motions, have been reported in the literature. It is probable that all the phenomena known for general dynamic systems occur also for particulate flows.

Levitation to equilibrium of 300 circular particles.

The transport of a slurry of 300 heavier than liquid particles in a plane pressure driven flow was studied using DNS in Choi and Joseph (2001). Time histories of fluidization of the particles for three viscous fluids with viscosities η = 1, 0.2 and 0.01 (water) were computed at different pressure gradients. The study leads to the concept of fluidization by lift in which all the particles are suspended by lift forces against gravity perpendicular to the flow.

The time history of the rise of the mean height of particles at a given pressure gradient is monitored and the rise eventually levels off when the bed is fully inflated. The time taken for full inflation decreases as the pressure gradient (or shear Reynolds number) increases (see Figure 8). At early times, particles are wedged out of the top layer by high pressure at the front and low pressure at the back of the particle in the top row (t = 1 in Figure 8a, t = 0.9 in Figure 8b).

The dynamic pressure at early times basically balances the weight of the particles in the rows defining the initial cubic array. This vertical stratification evolves into a horizontally stratified propagating wave of pressure, which tracks waves of volume fraction. The pressure wave is strongly involved in the lifting of particles. For low viscosity fluids like water where R_G is large the particle-laden region supports an "interfacial" wave corresponding to the wave of pressure. If R^2/R_G is large the interface collapses since the stronger lift forces push wave crests into the top of the channel, but the pressure waves persist (Figure 9).

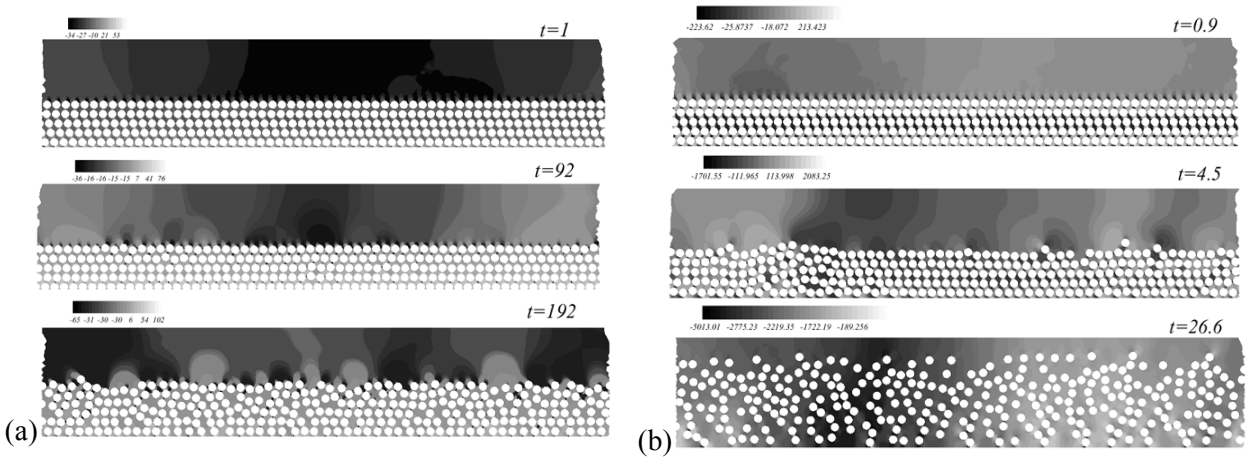

*Figure 8. (Choi and Joseph 2001.) (a) Snapshots of the fluidization of lift of 300 circular particles ρ_p = 1.01 g/cm^3 when η = 1 poise (*R = 5.4, R^2/R_G = 1.82). *The flow is from left to right. The gray scale gives the pressure intensity and dark is for low pressure. At early times particles are wedged out of the top layer by high pressure at the front and low pressure at the back of each and every circle in the top row. The vertical stratification of pressure at early times develops into a "periodic" horizontal stratification, a propagating pressure wave. The final inflated bed has eroded, rather tightly packed at the bottom with fluidized particles at the top. (b) Fluidization of 300 particles (*R = 120, R^2/R_G = 0.08). *The conditions are the same as in 9(a) but the ratio of lift to buoyant weight is greater and the fluidization is faster and the particle mass center rises higher than in the previous Figures.*

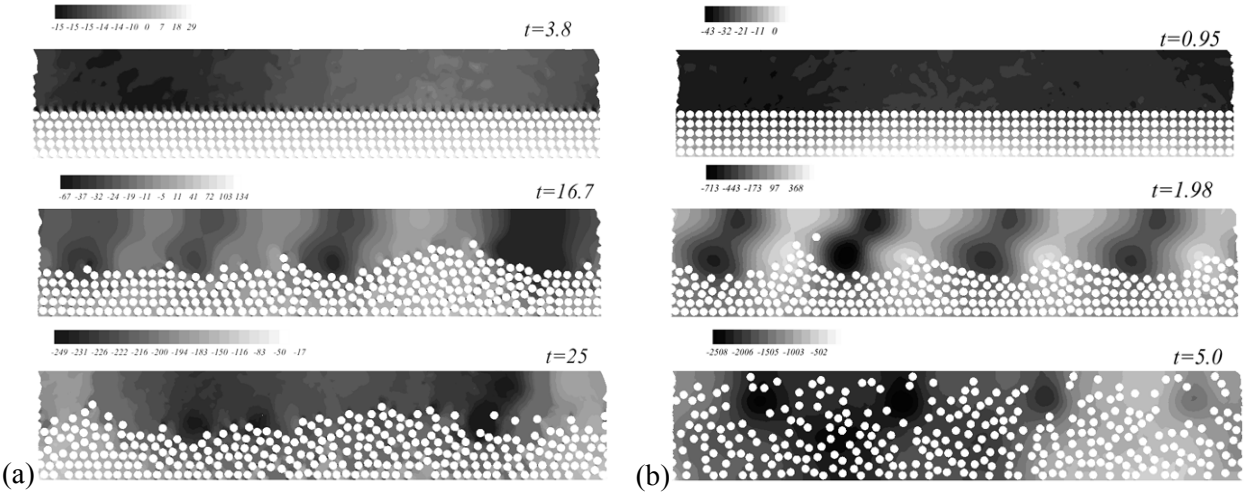

Figure 9. (Choi and Joseph 2001.) (a) Fluidization of 300 particles (η = 0.2 poise, R = 150, R^2/R_G = 1.63). *The final state of the fluidization at* t = 25 sec *has not fully eroded. The particles that lift out of the bed can be described as saltating. A propagating "interfacial" wave is associated with the propagating pressure wave at* t = 25. *(b). Fluidization of 300 particles (η = 0.2 poise,* R = 450, R^2/R_G =0.54). *The flow is from left to right. The particles can be lifted to the top of the channel.*

We did correlations in numerical experiments in 2D. Correlations work. We studied the levitation of 300 particles in a Poiseuille flow, Patankar, Ko, Choi and Joseph (2000), Choi and Joseph (2001), and created a data bank which when plotted on a log-log plot give rise to straight lines; this is to say that lift results for fluidized slurries are power laws in appropriate dimensionless parameters. This shows that fluidization of slurries by lift also falls into enabling correlations of the RZ type. The method of correlations is a link between direct simulation and engineering application.

Correlations allow generalizations from 20 or 30 data points into a continuum of points reaching even beyond where we can compute. Because you get so much from correlations even expensive calculations are cheap.

The correlation we found for lift-off of a single particle is in the form

$$R_G = aR^n, \quad a = 2.36, \qquad n = 1.39 \tag{8}$$

where R and R_G are defined by (5); a and n are obtained by plotting about 25 data points in a log R vs. log R_G plane (Patankar, Huang, Ko and Joseph (2001), Figure 10). The straight lines that come out are amazing; they show that self-similarity lies at the foundation of solid-liquid flows. Similar correlations were found for lift-off in viscoelastic fluids Ko, Patankar and Joseph (2001), Patankar, *et al* (2001) (Figure 11).

For 300 particles in Poiseuille flow we processed simulation data for the rise of the center of gravity of particles in the slurry; from the height rise we can compute the solid fraction ϕ. Processing data in log-log plots (Figure 12) we got

$$R_G = 3.27 \times 10^{-4} (1-\phi)^{-9.05} R^{1.249} \tag{9}$$

This could be called a Richardson-Zaki type of correlation for fluidization by lift Patankar, Ko, Choi and Joseph (2001).

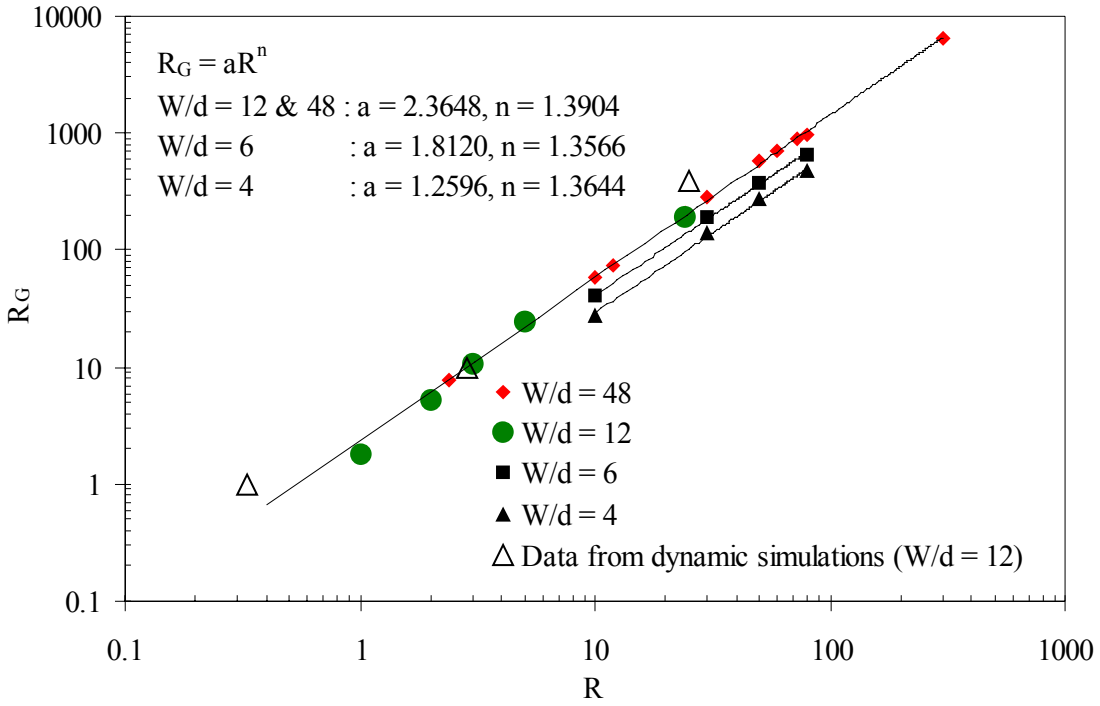

Figure 10. (Patankar, Huang, Ko and Joseph 2001.) The plot of R_G *vs. the critical shear Reynolds number* R *for lift-off on a logarithmic scale at different values of the channel width/diameter ratio* W/d. *This has evidently reached its asymptotic* $W/d \to \infty$ *value when* $W/d = 12$.

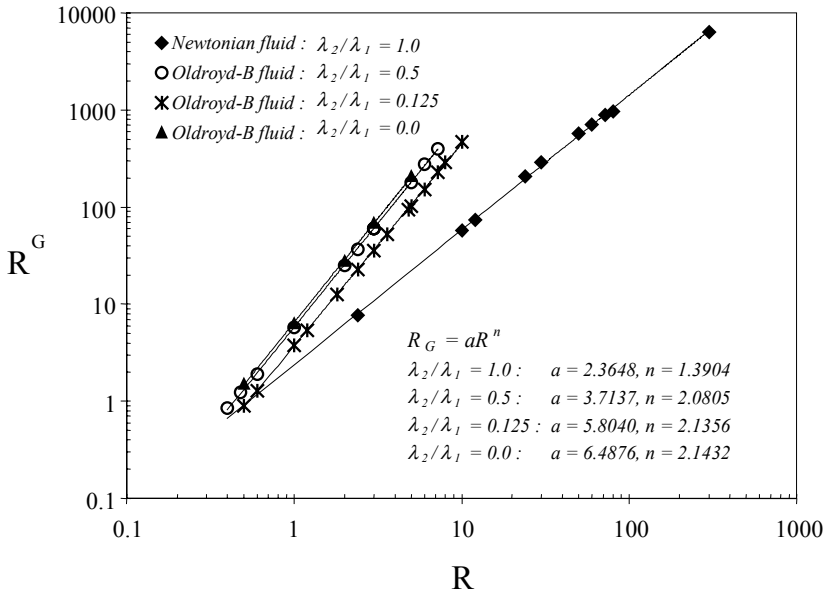

Figure 11. (Ko, Patankar and Joseph 2001.) RG vs. R for lift-off of an Oldroyd B fluid with different relaxation/ retardation time ratios in a log-log plot (W/d = 12, elasticity E = l1h/rfd2.)

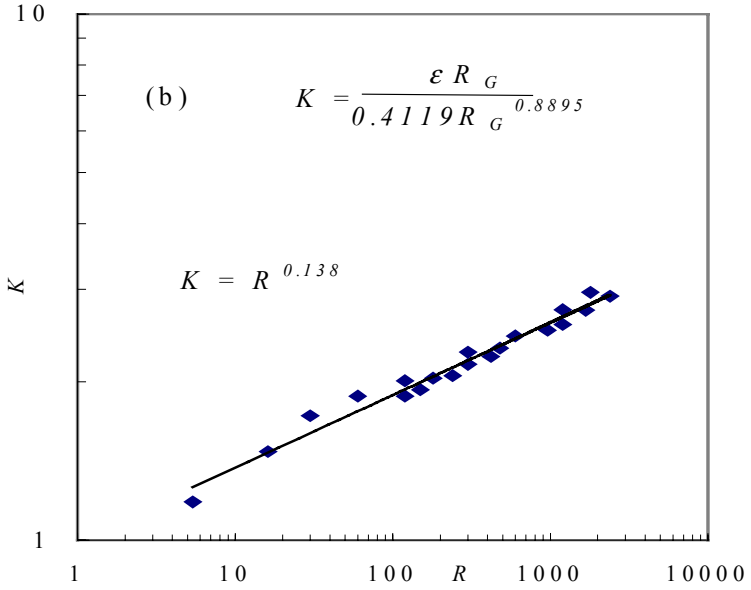

*Figure 12. (Patankar, Huang, Ko and Joseph 2001.) An engineering correlation (9) for lift-off from numerical simulations of 300 circular particles in plane Poiseuille flows of Newtonian fluids (*W/d = *12).*

Engineering correlations

We have already demonstrated that two-dimensional simulations of solid liquid flows give rise to power laws. These power laws are in the form of engineering correlations; to use them in applications we need rules for converting two- to three-dimensional results. The goal of our future work is to generate power laws for engineering applications by processing results of simulations in 3D just as we have done in 2D. The processing of data for the fluidization of 1204 spheres from a simulation and experiment which leads to comparison in Figure 2 is an example of what can be done.

We are presently doing 3D simulations for lift-off and levitation to equilibrium of single spheres and enhancing our simulators for efficient computation of migration and lift of slurries of many spherical particles. These simulators will be used to generate power laws for practical application to sand transport in fractured reservoir, among others.

Sand transport in fractured reservoirs.

Hydraulic fracturing is a process often used to increase the productivity of a hydrocarbon well. A slurry of sand in a highly viscous, usually elastic, fluid is pumped into the well to be stimulated, at sufficient pressure to exceed the horizontal stresses in the rock at reservoir depth. This opens a vertical fracture, some hundreds of feet long, tens of feet high, and perhaps an inch in width, penetrating from the well bore far into the pay zone. When the pumping pressure is removed, the sand acts to prop the fracture open. Productivity is enhanced because the sand-filled fracture offers a higher-conductivity path for fluids to enter the well than through the bulk reservoir rock, and because the area of contact for flow out from the productive formation is increased. It follows that a successful stimulation job requires that there be a continuous sand-filled path from great distances in the reservoir to the well, and that the sand is placed within productive, rather than non-productive, formations.

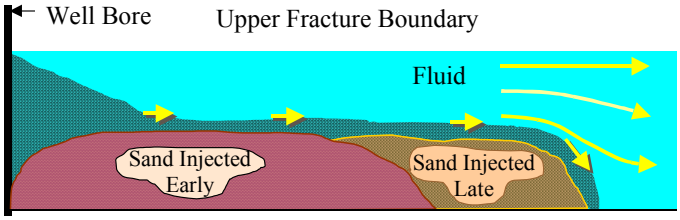

Figure 13. (Kern, Perkins and Wyant 1959) Sand transport in a fractured reservoir is different than the eroded bed of 300 particles in Figure 9(a) and 10(a) because particles are injected. The creation of algorithms to simulate continuous injection is one of our simulation projects.

In a slot problem a particle laden (say 20% solids) fluid is driven by a pressure gradient and the particles settle to the bottom as they are dragged forward. Sand deposits on the bottom of the slot; a mound of sand develops and grows until the gap between the top of the slot and the mound of sand reaches an equilibrium value; this value is associated with a critical velocity. The velocity in the gap between the mound and the top of the slot increases as the gap above the mound decreases. For velocities below critical the mound gets higher and spreads laterally; for larger velocities sand will be washed out until the equilibrium height and velocity are reestablished (see Figure 13). The physical processes mentioned here are *settling* and *washout*. Washout could be by sliding and slipping; however, a more efficient transport mechanism is by *advection after suspension* which we studied by direct simulation.

Despite many years of practice and experiments many of the most essential fluid dynamic properties of proppant transport, other than fluidization by lift, are not well understood. To help our studies of these properties be focused and practical, we have partnered with STIM-LAB, a research laboratory in Duncan, OK, which is supported by a consortium of oil production and oil service companies. STIM-LAB has been collecting data on sand transport in slots for 15 years. We have begun to process the data from STIM-LAB's experiments for power laws in the same way we process data form numerical simulations. An example is given just below.

Power law for bed erosion.

STIM-LAB carried out two types of experiments looking at the transport of proppants in thin fluids. The first experiment can be described as a lift-off or erosion experiment. A somewhat simplified description of the experiment is that a bed of proppant is eroded by the flow of water. Proppant is not injected. The faster the flow of water the deeper is the channel above. We are seeking to predict the height above the channel.

The evolution of the proppant bed in the experiments is well described in the diagram of Figure 13 with the caveat that experimental cell has a finite length. In the steady state there is an initial development

length followed by a flat bed that is divided into zones shown in Figure 14. The bottom of the bed is immobile, it is a stationary porous media that supports liquid throughput that might be modeled by Darcy's law. Above the immobile bed is a mobile bed in which particle slide and roll but do not lift. The traction carpet is a fully fluidized bed in which particles move forward in free motion under a balance of buoyant weight and lift. The lift off region lies between the stationary and fluidized bed.

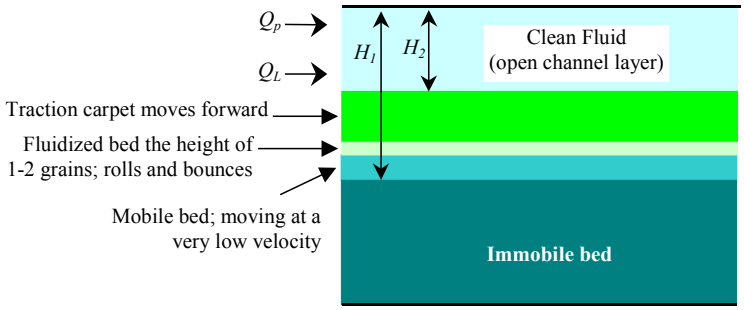

Figure 14. Proppant transport in thin fluid at steady state conditions. In the erosion experiments only fluid is pumped, $Q_P = 0$, $H_1 = H_2$, the particles don't move and H_2 is determined by Q_P.

The slot used in the erosion experiments was 8' long, 2' high and 3/16" wide; friction from the close side walls is most important in the slot and in real fractures. The open channel zone is defined by the presence of a channel, or proppant-free conduit, above the proppant pack. This zone comprises most of the length of the model and probably is also the dominant zone in a fractured well. Proppant moves in response to the shear stress generated by the moving fluid in the channel. In summary, the channel base is eroded until an equilibrium height is reached for a given velocity. If velocity decreases, the channel is stable. If velocity increases, the channel depth increases. Most sand erosion and transport is from this zone.

In the experiment, flow was established through the slot, causing proppant to erode from the top of the pack and a channel to form. Once a channel formed above the proppant it was allowed to equilibrate at least until the lower plane bedforms dominated the length of the slot. If necessary, the flow rate was then reduced until no there was no movement of proppant in the channel. When no proppant movement was detected along the channel base, the flow rate, channel height, differential pressures, and temperatures were recorded. The flow rate was then increased and the procedure repeated to generate the data in Table 1; the nomenclature for this table is given just below.

The processing for power laws in our 2D simulations were framed in terms of a Reynolds number for the forward flow

$$R = Vd/\eta \tag{10}$$

and a sedimentation "Reynolds number" based on the settling velocity $\dfrac{\rho_f(\rho_p - \rho_f)gd^2}{\eta}$ in Stokes flow.

$$R_G = \rho_f \frac{(\rho_p - \rho_f)gd^3}{\eta^2} \tag{11}$$

The fluid velocity V is related to the pressure drop across the flow cell.

Proppants	d (cm)	H_2 (cm)	η (gm/cm•s)	ρ_f (gm/cc)	υ (cm^2/s)	Q (cc/s)	ρ_p (gm/cc)	R_G	$\widetilde{V}$ (cm/s)	$\widetilde{R}$	H_2/W
	0.034212	1.7	0.01115	0.999	0.011161	36.778	2.65	521.1645	58.37416	178.9337	2.141732
60/40	0.034212	2.3	0.01115	0.999	0.011161	58.289	2.65	521.1645	92.51649	283.5899	2.897638
Brady	0.034212	5.6	0.01115	0.999	0.011161	133.295	2.65	521.1645	211.5662	648.512	7.055118
	0.034212	7.8	0.01115	0.999	0.011161	232.588	2.65	521.1645	369.1644	1131.596	9.826772
	0.056043	2.3	0.01115	0.999	0.011161	46.556	2.65	2290.822	73.89383	371.0382	2.897638
20/40	0.056043	5.2	0.01115	0.999	0.011161	133.106	2.65	2290.822	211.2663	1060.817	6.551181
Ottawa	0.056043	8.2	0.01115	0.999	0.011161	227.542	2.65	2290.822	361.1554	1813.446	10.33071
	0.06	1.4	0.01115	0.999	0.011161	7.885	1.05	86.83778	12.5151	67.27847	1.76378
20/40	0.06	2	0.01115	0.999	0.011161	10.409	1.05	86.83778	16.5212	88.8144	2.519685
Light	0.06	3.9	0.01115	0.999	0.011161	31.92	1.05	86.83778	50.66353	272.3562	4.913386
Beads	0.06	8.5	0.01115	0.999	0.011161	128.438	1.05	86.83778	203.8572	1095.892	10.70866
	0.06	12	0.01115	0.999	0.011161	226.217	1.05	86.83778	359.0523	1930.188	15.11811
	0.094946	1.5	0.01	0.998	0.01002	31.542	2.73	14513.72	50.06356	474.3833	1.889764
16/20	0.094946	2.2	0.01	0.998	0.01002	50.467	2.73	14513.72	80.10138	759.0103	2.771654
Carbolite	0.094946	9.9	0.01	0.998	0.01002	258.642	2.73	14513.72	410.5174	3889.907	12.47244
	0.094946	1.7	0.00378	0.972	0.003889	36.778	2.73	100415.8	58.37416	1425.188	2.141732
16/20	0.094946	2.3	0.00378	0.972	0.003889	58.289	2.73	100415.8	92.51649	2258.763	2.897638
Carbolite	0.094946	5.6	0.00378	0.972	0.003889	133.295	2.73	100415.8	211.5662	5165.329	7.055118
	0.094946	7.8	0.00378	0.972	0.003889	232.588	2.73	100415.8	369.1644	9013.043	9.826772
	0.088437	0.4	0.01115	0.999	0.011161	10.535	3.45	13363.76	16.72119	132.4925	0.503937
16/30	0.088437	0.6	0.01115	0.999	0.011161	13.878	3.45	13363.76	22.02721	174.5354	0.755906
Banrite	0.088437	1.3	0.01115	0.999	0.011161	29.145	3.45	13363.76	46.25904	366.5394	1.637795
	0.088437	3.5	0.01115	0.999	0.011161	100.681	3.45	13363.76	159.8012	1266.205	4.409449
	0.088437	8.3	0.01115	0.999	0.011161	261.796	3.45	13363.76	415.5234	3292.454	10.45669
	0.109021	1.3	0.01015	0.998	0.01017	28.955	2.65	20342.9	45.95747	492.643	1.637795
12/20	0.109021	2.5	0.01015	0.998	0.01017	62.137	2.65	20342.9	98.62404	1057.205	3.149606
Badger	0.109021	5.8	0.01015	0.998	0.01017	155.185	2.65	20342.9	246.3101	2640.332	7.307087
	0.109021	9	0.01015	0.998	0.01017	290.814	2.65	20342.9	461.5809	4947.936	11.33858

Table 1: Data set for lift-off experiments from Table 4.9.4.9-1 in Appendix 2

Nomenclature and scaling parameters

ρ_p density of the particles, gm/cm^3
d mean diameter of the particles, cm
ρ_f density of the fluid, gm/cm^3
η dynamic viscosity of the fluid, gm/cm-s
$\overline{p}$ average pressure gradient applied in the flow direction (if available), gm/(cm-s)^2
Q_f volumetric flow rate of the fluid, cm^3/s

(continues on next page)

Nomenclature and scaling parameters (continued)

M_p mass flow rate of the proppants, gm/s

Q_p volumetric flow rate of the proppants = M_p/ρ_p, cm3/s

Q_T total volumetric flow rate (fluid + proppant) = $Q_f + Q_p$, cm^3/s

h open channel height cm; (H_2)

H_1 see Figure 14, cm

H_2 see Figure 14, cm

W channel width 0.79375cm

A area cc; ($A = W * H_2$)

υ kinematic viscosity c^2/s; $\upsilon = \dfrac{\eta}{\rho_f}$

V fluid velocity cm/s; $V = \dfrac{Q}{A} = \dfrac{Q}{WH_2}$;

$\widetilde{V}$ fluid velocity cm/s; $\widetilde{V} = \dfrac{Q}{W^2}$;

R Reynolds number (based on V); $R = \dfrac{Vd}{\upsilon}$;

$\widetilde{R}$ Reynolds number (based on $\widetilde{V}$); $\widetilde{R} = \dfrac{\widetilde{V}d}{\upsilon} = \dfrac{RH_2}{W}$;

G gravity parameter; $G = \dfrac{(\rho_p - \rho_f)gd^2}{\eta V}$;

R_G gravity Reynolds number; $R_G = \dfrac{\rho_f(\rho_p - \rho_f)gd^3}{\eta^2} = GR$;

S Shields parameter is defined as: $S = \dfrac{\tau}{(\rho_p - \rho_f)gd}$;

If we take $\tau = \eta\dot{\gamma}_w$ and $V = \dot{\gamma}_w d$, then $S = \dfrac{\eta V}{(\rho_p - \rho_f)gd^2} = \dfrac{1}{G}$.

It is important to do correlations in terms of dimensionless parameters; this leads to maximum generality. To see this consider power laws, which we found, that are of the form

$$R_G = aR^n \tag{12}$$

for lift-off. For R larger than $(R_G)^{1/n}/a$, the particle of radius d and density ρ_p will levitate. This equation (12) may be written as

$$\rho_f \frac{(\rho_p - \rho_f)gd^3}{\eta^2} = a\left(\frac{Vd}{\eta}\right)^n \tag{13}$$

Suppose we did experiments for lift-off in a certain fluid with a given proppant of different size. We would find a correlation of the form

$$V = bd^m \tag{14}$$

We wouldn't know that $m = {}^3/_n - 1$ or how all the other parameters enter into the correlation.

Erosion experiments; for these experiments $H_1 = H_2$ and only water is moving.

STIM-LAB did experiments on bed erosion. These are essentially lift-off experiments since the flow rate is dropped to a critical lift-off value below which particles are not eroded from the bed.

In Table 1 we reformulate the data from the STIM-LAB experiments for processing in terms of R_G and

$$\widetilde{R} = \frac{\widetilde{V} d}{\nu} \tag{15}$$

where

$$\widetilde{V} = \frac{Q}{W^2} \tag{16}$$

and Q is the volume flow rate. We use $\widetilde{V}$ because Q and W are prescribed data.

There are seven groups in the data shown in Table 1; each one corresponds to a value of R_G. The data corresponding to a given R_G is ordered by increasing H_2; the larger R corresponds to a larger H_2 more or less, but there are exceptions.

Power fit:* H_2/W *vs.* $\widetilde{R}$ *in a log-log plot.

It is rather obvious that the height H_2 will increase with Q at a fixed R_G (for fixed proppant and fluid). With R_G fixed we can hope for a two-parameter correlation. In Figure 15 we show seven more or less straight lines for the seven values of R_G. The power law for these is given by

$$\frac{H_2}{W} = a(R_G)\, R^{m(R_G)} \tag{17}$$

where $a(R_G)$ and $m(R_G)$ are listed in Table 2. The value of the exponent $m(R_G) \approx 0.87$ for all cases except $R_G = 86.84$ corresponding to nearly neutrally buoyant particles ($\rho_p = 1.05$ gm/cc).

R_G	$a(R_G)$	$m(R_G)$
86.84	1.479E-1	0.6140
521.16	2.326E-2	0.8672
2290.822	1.700E-2	0.8600
13363.76	6.393E-3	0.9174
14513.72	6.40E-3	0.9170
20342.90	8.476E-3	0.8508
100415.72	3.847E-3	0.8672

Table 2. The coefficients (as functions of R_G*) used in power fit for* H_2/W.

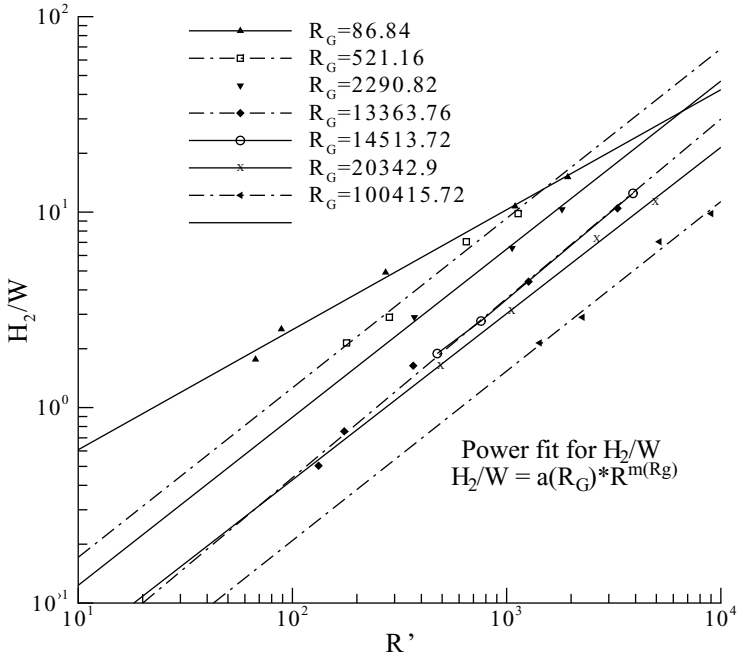

Figure 15. H_2/W *vs.* $\widetilde{R}$ *in log-log plot for different values of* R_G *(see Table 2).*

Inspection of Table 2 shows that when $R_G \geq 521$

$$m(R_G) \approx 0.87 \tag{18}$$

whereas when $R_G = 86.84$ ($\rho_p = 1.05$) we get

$$m(R_G) \approx 0.61\ . \tag{19}$$

This shows that the exponent m does depend on and we may hope to describe this dependence in intervals (as is true for the Richardson-Zaki $n(R)$, which depends in intervals on the Reynolds number R). For example, we could suppose that there is a certain value of $R_G = R_{GC}$ for which the $m(R_G)$ take on the two values, (18) if $R_G > R_{GC}$ and (19) is $R_G < R_{GC}$ where $86.84 \leq R_{GC} \leq 521.16$.

Summarizing we may propose

$$\frac{H_2}{W} = a(R_G)\, R^{m(R_G)} \tag{20}$$

where $m(R_G)$ are given approximately by (18) and (19).

The final correlation* $\mathbf{a(R_G)}$ *as* $\mathbf{R_G}$ *in a log-log plot.

We plotted $a(R_G)$ as given in Table 2 against R_G in a log-log plot. This plot is shown in Figure 16 and gives rise to the formula

$$a = 0.8007\ R_G^{\ -0.4854}\ . \tag{21}$$

For the coefficient $a(R_G)$

$$a(R_G) = b \times R^k{}_G\ .$$

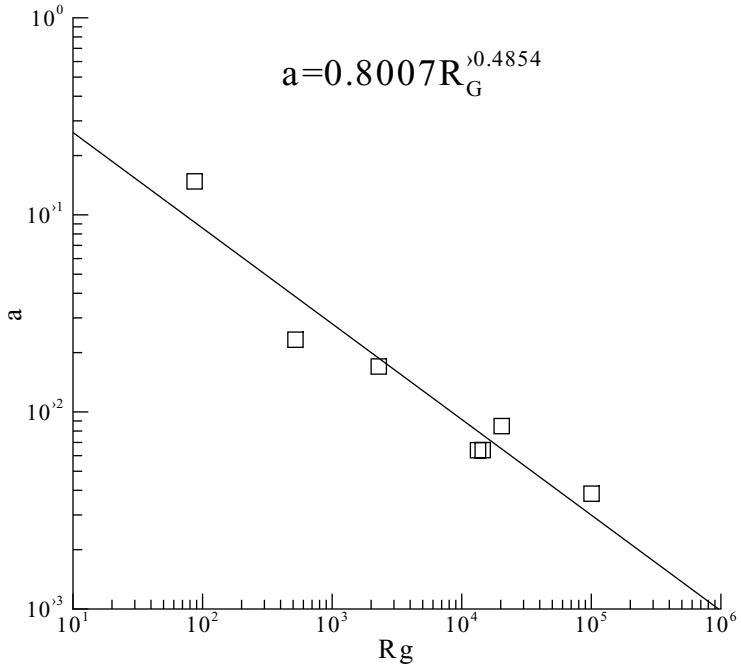

Figure 16. Power fit for $a(R_G)$ *vs.* R_G.

Combining now (20) and (21)

$$\frac{H_2}{W} = 0.8007 \times R_G^{-0.4854} \times \widetilde{R}^{m(R_G)} \tag{22}$$

where $m(R_G) \approx 0.87$ for $R_G > R_{GC}$, where $86 < R_{GC} < 500$ and $m \approx 0.614$ for $R_G < R_{GC}$.

We are proposing (22) as a widely applicable correlation for lift-off valid beyond where data has already been taken. More experiments, testing (22) validity for different values of W under more extreme conditions ought to be undertaken; of particular interest are light particles for which $R_G < R_{GC}$.

When $R_G > R_{GC}$ we can write (22) as

$$\frac{H_2}{W} = 0.8007\left[\frac{\rho_f(\rho_p - \rho_f)gd^3}{\eta^2}\right]^{-0.4854}\left(\frac{\rho_f Qd}{W^2\eta}\right)^{0.87} \tag{23}$$

Equation (23) gives the fracture height in terms of given quantities. Formula (22) can be expressed in terms of the Shield's parameter $1/G$ by writing $\widetilde{R} = \frac{R_G H_2}{GW}$.

Conclusions

We believe that research leading to optimal techniques of processing data for correlations from real and numerical experiments is founded on the far from obvious property of self similarity (power laws) in the flow of dispersions. The bases for this belief are the excellent correlations of experiments on fluidization and sedimentation done by Richardson and Zaki and the correlations for lifting of slurries in horizontal conduits obtained form numerical experiments described here. The method of correlations is a new link between DNS and engineering practice.

Results of two dimensional simulations of solid-liquid flows give rise to straight lines in log-log plots of the relevant dimensionless Reynolds numbers. The extent and apparent universality of this property is remarkable and shows that the flow of these dispersions are governed by a hidden property of self similarity leading to power laws. These power laws make a powerful connection between sophisticated high performance computation and the practical world of engineering correlations. The same methods for processing data are applied to numerical and real experiments.

The Richardson-Zaki correlation is of great relevance in seeing the image of the future. The power law in the RZ case is an example of what Barenblatt (1996) calls "incomplete self similarity" because the power itself depends on the Reynolds number, a third parameter. The three parameter bed erosion correlation (22) is an example of the kind of correlation we expect to emerge from 3D simulations. More generally we expect that the processing of real data from both real and numerical experiments will lead to families of straight lines in log-log plots connected by transition regions.

Acknowledgment

This work was partially supported by the National Science Foundation DKI/New Computational Challenge grant (SNF/CTS 98-73236), by the DOE, Department of Basic Energy Sciences, by a grant from the Schlumberger foundation, from STIM-LAB Inc. and by the Minnesota Supercomputer Institute.

References

Papers marked with ♦ have been written in the last year and have not yet been published; they can be found and downloaded from our web site, *http://www.aem.umn.edu/Solid-Liquid_Flows/references.html*.

G.I. Barenblatt 1996. *Scaling, Self Similarity and Intermediate Asymptotics*. Cambridge Univ. Press.

H.G. Choi and Daniel D. Joseph, 2001. Fluidization by lift of 300 circular particles in plane Poiseuille flow by direct numerical simulation, accepted by *J. Fluid Mech*. ♦

D.D. Joseph, D. Ocando and P.Y. Huang, 2001. Slip velocity and lift, accepted by *J. Fluid Mech*. ♦

T.K. Kern, T.K. Perkins and R.E. Wyant 1959. The mechanics of sand movement in fracturing, Petroleum Transactions, AIME 216, 403-405.

T. Ko, N.A. Patankar and D.D. Joseph 2001. Lift-off of a single particle in an Oldroyd-B fluid. Submitted to *Phys. Fluids*.

N.A. Patankar, T. Ko, H.G. Choi and D.D. Joseph, 2001. A correlation for the lift-off of many particles in plan Poiseuille of Newtonian fluids, accepted by *J. Fluid Mech*. ♦

N.A. Patankar, P.Y. Huang, T. Ko and D.D. Joseph, 2001. Lift-off of a single particle in Newtonian and viscoelastic fluids by direct numerical simulation, accepted by *J. Fluid Mech.*.

T.-W. Pan, D.D. Joseph, R. Bai, R. Glowinski and V. Sarin, 2001. Fluidization of 1204 spheres: simulation and experiment, *J. of Fluid Mech*. to appear. ♦

J.F. Richardson and W.N. Zaki, 1954. Sedimentation and Fluidization: Part I, *Trans. Instn. Chem.* Engrs. **3**2, 35–53.